TIME DOMAIN MODELING OF COMPLIANT WORKPIECE MILLING

Mark A. Rubeo and Tony L. Schmitz
Mechanical Engineering and Engineering Science
University of North Carolina at Charlotte
Charlotte, NC

INTRODUCTION

High performance application areas, such as the energy production, power, and aerospace industries, benefit from the enhanced product quality and reduced cost associated with machining thin-walled, metallic structures over the traditional fabrication and assembly methods. A methodology for machining compliant aluminum workpieces, described in [1-3], has been established and has become prevalent in the aerospace industry. The manufacturing strategy for these components consists of selectively removing material, via high-speed machining, from a solid billet to yield a monolithic component [4].

The superior mechanical properties of difficult-to-machine materials, such as titanium and nickel alloys, make them ideal candidates for compliant, thin-walled structures. However, the same machining methodology that has been applied to aluminum is not appropriate for these materials due to their excessive cost and limitations imposed by tool wear [5]. Near net shape techniques have been used to manufacture compliant structures composed of hard-to-machine materials, but these techniques are often unable to achieve the required dimensional tolerances. Because of the inherent compliance of the preforms, stable machining is difficult to achieve. Prediction of stable machining parameters is critical for the finish machining of such compliant workpieces.

The aim of this study is to evaluate the stability of milling operations where the workpiece is considerably more compliant than the machine-tool system. The evaluation is performed by implementing peak-to-peak (PTP) force diagrams as described in [6]. These diagrams result from multiple time domain simulations (TDS) completed over a range of spindle speeds and axial depths of cut. The outcome of an individual time domain simulation contains information specific to the spindle speed-axial depth of cut combination (i.e., cutting force, tool/workpiece deflection), while the PTP force diagrams contain the global information provided by a stability lobe diagram. By proper choice of spindle speed and axial depth of cut according to the PTP force diagrams, stable machining parameters may be selected.

In this paper, we describe the time domain simulation model used in this study including the mechanistic force model and Eulerian integration approach to solving the dynamic equations of motion. The applicability of the simulation is validated through milling experiments where stability predictions are made based on pre-process knowledge of the tool/workpiece dynamics and cutting forces. Simulated preforms are machined in order to illustrate the process and show typical results. The conclusions summarize the usefulness of the simulation and highlight further work being conducted to improve the predictive capabilities of the model.

TIME DOMAIN SIMULATION MODEL

Based on the “Regenerative Force, Dynamic Deflection Model” described in [6-9], the time domain simulation determines the instantaneous chip thickness, calculates cutting forces, and uses Euler (fixed time step numerical) integration of the equations of motion to determine tool/workpiece deflections at each incremental time step. It is able to account for the nonlinearity which occurs during the milling process when the deflection of the tool/workpiece become large enough that contact is lost [10]. The underlying assumptions built into the model include the circular tool path approximation and a mechanistic force model [11].

The instantaneous chip thickness depends on the feed per tooth, the relative vibration of the tool/workpiece in the surface normal direction for the current and previous cutting teeth, and cutter runout. Therefore, instantaneous chip thickness is expressed as:

$$h(t) = f_t \sin(\varphi) - n(t-\tau) - n(t) + r \qquad (1)$$

where $f_t \sin(\varphi)$ is the nominal, tooth angle dependent chip thickness, $n(t-\tau)$ is the relative vibration of the tool/workpiece in the direction of the surface normal of the previous tooth, $n(t)$ is the current, relative vibration of the tool/workpiece in the normal direction, and r is the cutter runout. In these expressions, f_t is the feed per tooth, φ is the cutter rotation angle, t is the current time, and τ is the tooth passing period.

Cutting force calculations are based on the mechanistic force model presented by Budak et al. [11] and augmented with a process damping force [12]. At each incremental time step, the chip thickness is evaluated and, in the case where the tool has vibrated out of the cut (i.e., chip thickness is found to be less than or equal to zero), the instantaneous tangential, radial, and axial cutting forces are set to zero. For the case where the instantaneous chip thickness is non-zero, the instantaneous tangential, radial, and axial cutting forces can be expressed, respectively, as:

$$F_t^{i+1} = K_{tc} b h^{i+1} + K_{te} b - C_t b \frac{\dot{r}^i}{V} \qquad (2)$$

$$F_r^{i+1} = K_{rc} b h^{i+1} + K_{re} b - C_r b \frac{\dot{r}^i}{V} \qquad (3)$$

$$F_a^{i+1} = K_{ac} b h^{i+1} + K_{ae} b \qquad (4)$$

where b is the axial depth of cut and h^{i+1} is the instantaneous chip thickness for the current time step. K_{tc}, K_{rc}, and K_{ac} are the tangential, radial, and axial specific cutting force coefficients, respectively, which are associated with "cutting" or shearing. The tangential, radial, and axial edge force coefficients, K_{te}, K_{re}, and K_{ae}, capture the ploughing effect which occurs at small chip thicknesses. The expressions $C_t b \frac{\dot{r}^i}{V}$ and $C_r b \frac{\dot{r}^i}{V}$ are the process damping forces in the tangential and radial directions, respectively, where C_t and C_r are the tangential and radial process damping coefficients, $\dot{r}^i$ is the velocity in the radial direction calculated in the previous time step, and V is the cutting speed. These instantaneous cutting forces are then transformed into coordinate system shown in Fig. 1.

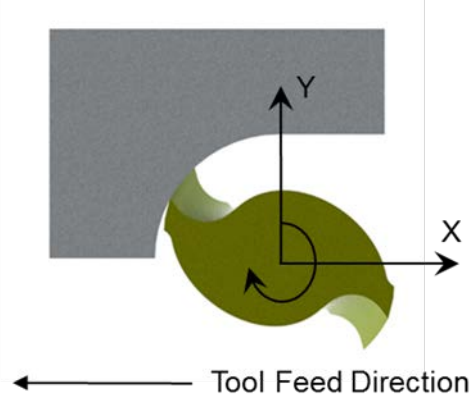

FIGURE 1. Coordinate system definition for the time domain simulation model. A down milling configuration is shown.

The equations of motion are solved in modal coordinates using Euler integration. The dynamics of the tool and workpiece are represented using modal parameters for an arbitrary number of degrees of freedom. The tool dynamics are considered in two orthogonal directions in the plane of the cut and the workpiece dynamics are considered in all three orthogonal directions. In modal coordinates the dynamic equation of motion may be expressed as:

$$F_q^i = m_q \ddot{q}^i + c_q \dot{q}^i + k_q q^i. \qquad (5)$$

Then, as an approximated solution for velocity, $\dot{q}^{i+1}$, and displacement, q^{i+1}, via Euler integration:

$$\ddot{q}^{i+1} = \frac{\left(F_q^i - c_q \dot{q}^i - k_q q^i\right)}{m_q} \qquad (6)$$

$$\dot{q}^{i+1} = \dot{q}_i + \ddot{q}^{i+1} \Delta t \qquad (7)$$

$$q^{i+1} = q^i + \dot{q}^{i+1} \Delta t \qquad (8)$$

where m_q, c_q, and k_q are the mass, damping, and stiffness values, respectively, expressed in modal coordinates, and Δt is the time step.

Additionally, the simulation model allows for a variety of tool geometries including an arbitrary number of cutting teeth, variable teeth spacing, different helix angles for each tooth, and cutter teeth runout. As a practical consideration it is

important to select a time step which is sufficiently small that the Euler integration method provides a numerically stable solution. A rule of thumb is that the time step should be at least ten times smaller than the period associated with the highest oscillation frequency present in the system being modeled. Also, the number of time steps (i.e., cutting tool revolutions) should be sufficiently high for the initial transient behavior to decay.

As previously mentioned, the outcome of individual time domain simulations contains information specific to the individual spindle speed-axial depth of cut combinations. This includes the instantaneous cutting forces and tool/workpiece deflections, velocities, and accelerations. The PTP force diagrams represent numerous time domain simulations performed over a range of spindle speed-axial depth of cut combinations. The range and step size of the spindle speed and axial depth of cut is specified, and the time domain simulation is performed for each combination. At the conclusion of each simulation the steady state portion of the time domain cutting forces are examined for the maximum peak-to-peak (PTP) force difference. The PTP force for each combination of spindle speed and axial depth of cut is used to generate a contour map over the range of spindle speeds and axial depth of cuts. The result is analogous to the traditional stability lobe diagram in the sense that it conveys a global representation of stable and unstable spindle speed and axial depth of cut combinations while retaining the specific, local information of the individual combinations.

EXPERIMENT DESCRIPTION

To validate the time domain simulation model, experiments were conducted. The cutting tests were performed on compliant workpieces, shown in Fig. 2, which simulate near net shape components. These compliant workpieces were machined from 6061-T651 aluminum and are composed of two thin-walled structures with clamped-clamped-clamped-free (CCCF) boundary conditions. The geometric dimensions of the thin-walled structures, or ribs, are given in Table 1.

FIGURE 2. Model of the compliant workpiece.

The cutting tool used for the validation experiments was a 12.7 mm carbide end mill with two flutes, evenly spaced, and a 30º helix angle. Modal parameters for the tool were obtained via impact testing using an instrumented hammer (PCB 086C04) to provide the excitation force and a low mass accelerometer (PCB 352C23) to record the response. Table 2 lists the natural frequency, f_n, modal stiffness, k, and damping ratio, ζ, for the dominant modes in the plane of the cut (i.e., X-Y).

TABLE 1. Geometry of individual ribs.

Length	Height	Thickness
130 mm	15 mm	1.5 mm

Since cutting forces were used as the primary metric by which the simulation model was validated, the workpiece was bolted to a cutting force dynamometer (Kistler 9257B) during impact testing, as shown in Fig. 3, to properly represent the workpiece dynamics during the validation tests. An instrumented hammer (PCB 084A17) was used to provide the excitation force and the workpiece response was measured using a non-contact laser vibrometer (Polytec OFV-534). Table 3 lists the natural frequency, f_n, modal stiffness, k, and damping ratio, ζ, for the two modes in the direction of greatest compliance (i.e., Y direction).

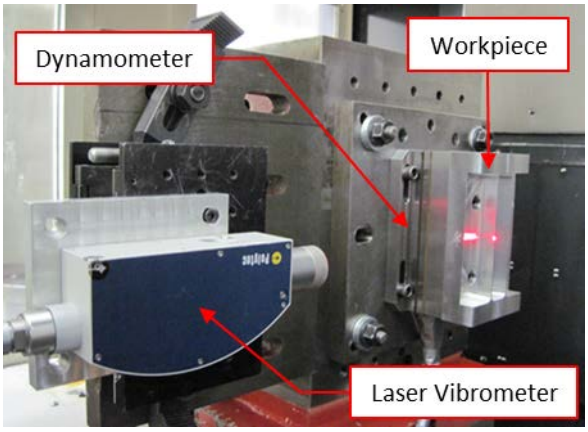

FIGURE 3. Impact testing setup for the compliant workpiece.

TABLE 2. Modal parameters for the cutting tool.

X direction		
$f_n\ [Hz]$	$k\ [N/m]$	ζ
2265	3.11×10^7	0.034
Y direction		
$f_n\ [Hz]$	$k\ [N/m]$	ζ
2254	3.09×10^7	0.027

The specific force coefficients used to calibrate the mechanistic force model applied in the time domain simulation were calculated using a constrained, least squares optimization method similar to the technique described in [13]. This method fits a set of simulated, instantaneous cutting forces to a set of measured, instantaneous cutting forces by iteratively updating the specific force coefficients until the convergence criteria is met. Table 4 lists the six specific force coefficients used in the simulation validation test.

TABLE 3. Modal parameters for rib.

Rib 1			
Mode	$f_n\ [Hz]$	$k\ [N/m]$	ζ
1	5837	1.59×10^6	0.0007
2	7787	4.17×10^6	0.0008

TABLE 4. Specific force coefficients for the simulation validation test.

Cutting force coefficients		
$k_{tc}\ [N/m^2]$	$k_{rc}\ [N/m^2]$	$k_{ac}\ [N/m^2]$
1119	322	305
Edge force coefficients		
$k_{te}\ [N/m]$	$k_{re}\ [N/m]$	$k_{ae}\ [N/m]$
2	0	0

The simulations were performed at 2% radial immersion in a down milling configuration with a commanded feed rate of $0.1\ \mathrm{mm/tooth}$. Flute-to-flute runout was specified as $3\ \mu\mathrm{m}$.

The PTP force diagram used in this validation study was generated over a spindle speed range from $7000\ \mathrm{rpm}$ to $9000\ \mathrm{rpm}$ at increments of $50\ \mathrm{rpm}$, and the axial depth of cut ranged from $0\ \mathrm{mm}$ to $0.6\ \mathrm{mm}$ in increments of $0.1\ \mathrm{mm}$. Computation time was approximately 5 minutes for the simulation. The PTP force diagram for the rib, shown in Fig. 4, was used to select a spindle speed-axial depth of cut combination at which to perform a validation test. A stable cut, as predicted by the simulation, was chosen. A comparison of the simulated and measured, instantaneous cutting forces are provided in the following section.

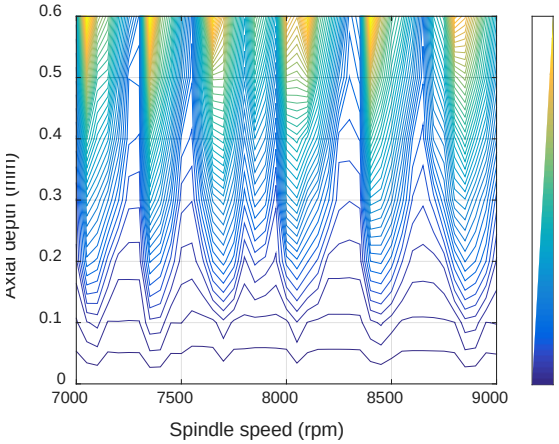

FIGURE 4. PTP force diagram indicating the selected, stable test point for rib 1 (the color bar indicates force in N).

EXPERIMENT RESULTS

The X direction cutting forces measured during the validation test, which was performed at a spindle speed of 8275 rpm and an axial depth of cut of 0.4 mm, are shown in Fig. 5. It is observed that the measured and simulated cutting forces are in good agreement and the variation in the cutting force from one tooth engagement to the next, due to flute-to-flute runout, is also captured by the time domain simulation.

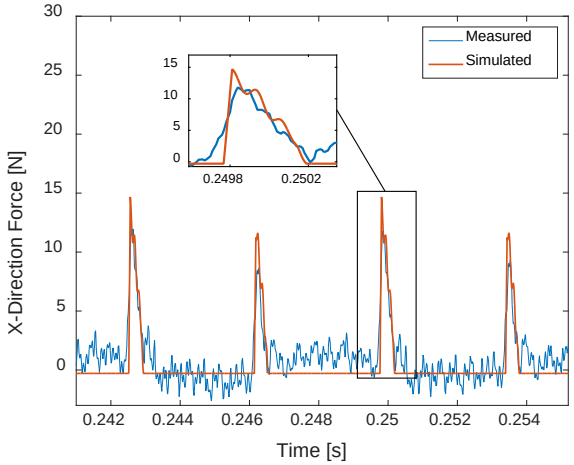

FIGURE 5. Measured and simulated X direction cutting forces shown for two cutter revolutions.

The frequency content of the X direction cutting force, computed using the Fast Fourier Transform (FFT), is shown in Fig. 6. It is observed that the dominant frequencies are the tooth passing frequency, 276 Hz, and the runout frequency, 138 Hz, as well as their integer multiples (i.e., harmonics). Some amplification of the frequency content near the rib's natural frequencies is also evident.

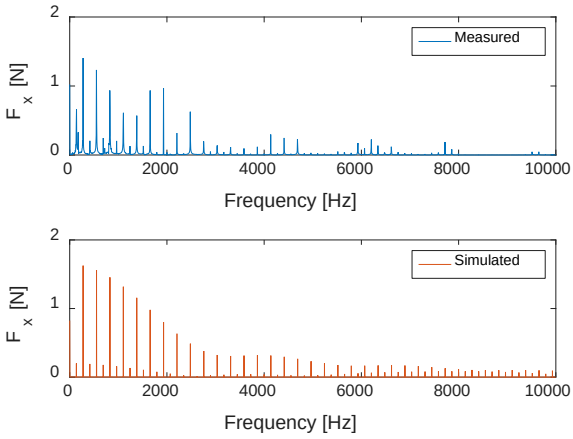

FIGURE 6. Frequency content of the measured and simulated X direction cutting forces.

The measured and simulated Y direction cutting forces, shown in Fig. 7, also exhibit good agreement in both peak amplitude and frequency content. See Fig. 8.

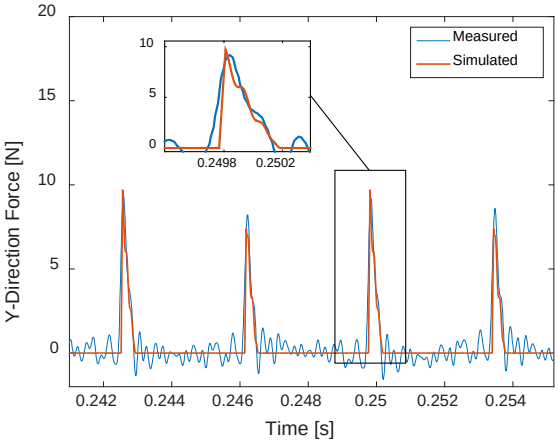

FIGURE 7. Measured and simulated Y direction cutting forces shown for two cutter revolutions.

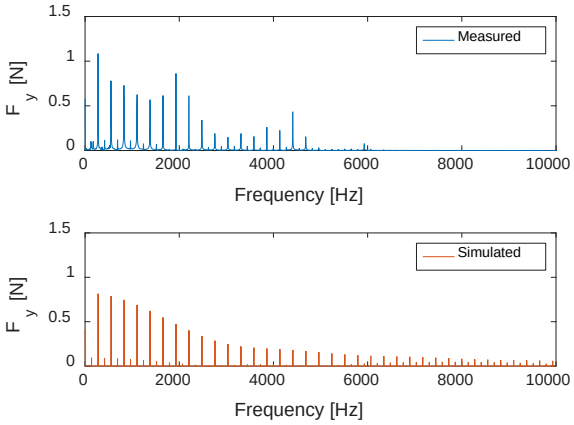

FIGURE 8. Frequency content of the measured and simulated Y direction cutting forces.

CONCLUSIONS

This paper presents the peak-to-peak force diagram and validates its applicability towards predicting stable and unstable conditions for compliant workpiece milling. The ability of the simulation to deliver the global stability predictions of traditional stability lobe diagrams has been demonstrated, and the specific, local information provided by the individual time domain simulations was validated.

For the purposes of milling compliant workpieces composed of hard-to-machine materials, the simulation model presented here may be augmented by including the process damping force. In the future, this work will be extended to include this force component to capture this stabilizing phenomenon at low speeds.

REFERENCES

[1] Tlusty J, Smith S, Winfough WR. Techniques for the Use of Long Slender End Mills in High-speed Milling. CIRP Annals - Manufacturing Technology. 1996; 45(1):393-6.

[2] Smith S, Winfough WR, Halley J. The Effect of Tool Length on Stable Metal Removal Rate in High Speed Milling. CIRP Annals - Manufacturing Technology. 1998; 47(1):307-10.

[3] Smith S, Dvorak D. Tool path strategies for high speed milling aluminum workpieces with thin webs. Mechatronics. 1998; 8:291-300.

[4] Halley J, Helvey A, Smith K, Winfough W, editors. The impact of high-speed machining on the design and fabrication of aircraft components. Proceedings of the 17th Biennial Conference on Mechanical Vibration and Noise, 1999 ASME Design and Technical Conferences, Las Vegas, Nevada, September 12-16, 1999.

[5] Smith S, Wilhelm R, Dutterer B, Cherukuri H, Goel G. Sacrificial structure preforms for thin part machining. CIRP Annals - Manufacturing Technology. 2012; 61(1):379-82.

[6] Smith S, Tlusty J. Efficient Simulation Programs for Chatter in Milling. CIRP Annals - Manufacturing Technology. 1993; 42(1):463-6.

[7] Schmitz TL, Smith KS. Machining dynamics: frequency response to improved productivity: Springer Science & Business Media; 2008.

[8] Smith S, Tlusty J. An overview of modeling and simulation of the milling process. Journal of engineering for industry. 1991; 113(2):169-75.

[9] Tlusty J. Manufacturing processes and equipment: Prentice Hall; 2000.

[10] Tlusty J, Ismail F. Basic Non-Linearity in Machining Chatter. CIRP Annals - Manufacturing Technology. 1981; 30(1):299-304.

[11] Budak E, Altintas Y, Armarego E. Prediction of milling force coefficients from orthogonal cutting data. Journal of Manufacturing Science and Engineering. 1996; 118(2):216-24.

[12] Tyler CT, Schmitz TL. Analytical process damping stability prediction. Journal of Manufacturing Processes. 2013; 15(1):69-76.

[13] Gonzalo O, Beristain J, Jauregi H, Sanz C. A method for the identification of the specific force coefficients for mechanistic milling simulation. International Journal of Machine Tools and Manufacture. 2010; 50(9):765-74.